UDC 343.982:681.183

Holographic Fingerprint Sensor

• Seigo Igaki • Shin Eguchi • Takashi Shinzaki

(Manuscript received November 10, 1989)

A sensor for personnel identification that uses a laser light source has been developed. It consists of a transparent light-conducting glass plate with a plain grating hologram, and a focusing lens under the hologram. Because the plate is plane-parallel, all optical paths from each point on the fingerprint to the hologram are equal, and a bright fingerprint image is obtained without the trapezoidal distortion inherent in prism sensors.

1. Introduction

Security continues to be an extremely important consideration in computer systems, and the ways in which it is implemented are legion. One popular way is the ID card, which provides efficient entry control to secure areas. However, cards can be lost or stolen. The use of a secret code is another efficient method of identification. It can be used, for example, to control the use of data entry terminals. But such codes can be easily guessed, especially in this age of personal computers and inventive hackers.

The fingerprint, being unique and unchangeable, remains the most reliable means of identification. A variety of ID and access control systems have been developed to identify users by fingerprint[1].

Such fingerprint identification systems must operate in realtime and use an algorithm that quickly compares an input with previously registered fingerprints.

Such systems must also produce distortion-free fingerprint images unaffected by latent fingerprint images.

2. Conventional sensors

Most fingerprint sensor use a prism (see Fig. 1) into which a beam is introduced through one of the prism's angled surfaces. The beam undergoes total internal reflection at the top of the prism. When a finger is placed on the prism, total internal reflection no longer occurs at the points of contact. Light incident at these points is not reflected, and a fingerprint image is imposed on the light reflected to the other angled surface. This image is then focused on the image pickup element (CCD) by a lens.

This method has two major problems:

1) Trapezoidal distortion caused by unequal optical paths between each point of the fingerprint and the image focusing lens.
2) Light noise caused by latent fingerprints.

A partial solution to these problems is shown in Fig. 2[2]. The image pickup element is positioned beyond the light scattered from fingerprint ridges. This improves the contrast and is effective against light noise, but does little to eliminate trapezoidal distortion.

To solve the above problems completely, we developed a holographic sensor[3] consisting of a plain grating hologram and a flat glass plate with a laser light source.

3. Holographic fingerprint sensor[3]

The transparent flat glass plate used in the holographic sensor has a hologram at one end and a fingerprint input port at the other (see Fig. 3). The laser beam is directed to the fingerprint input port from the back of the glass plate. The finger is simply pressed against the glass plate.

The sensor produces contrast by using the differences in the scattered light reflected

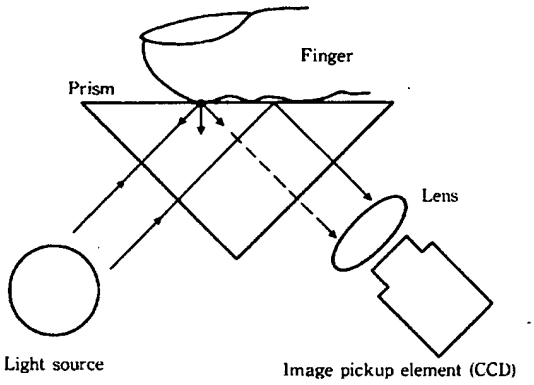

Fig. 1—Principle of prism fingerprint sensor-1.

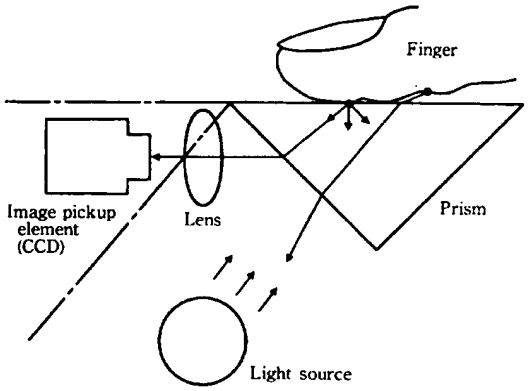

Fig. 2—Principle of prism fingerprint sensor-2.

in the glass from the fingerprint's grooves and ridges. Because of the thin layer of air between fingerprint grooves and the glass, the reflected light enters the glass from the air layer and then exits the other side at the angle of incidence. This reflected light enters the glass at different angles depending on how the fingerprint ridges touch the glass. Light entering at an angle of incidence below the critical angle is reflected repeatedly within the glass (total internal reflection) and propagates through the glass plate. Other light exits the glass in the same way as light scattered from a grooved surface. The repeatedly reflected light carrying the image of the fingerprint ridges exits the glass at the hologram. The external image-forming optical system then forms an image of the ridges.

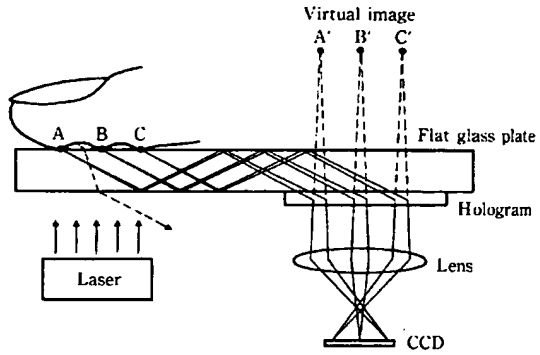

Fig. 3—Principle of holographic fingerprint sensor.

The parallel-plate of the holographic sensor equalize, all optical paths from the fingerprint to the hologram and eliminates trapezoidal distortion.

4. Designing the sensor optical system

4.1 Hologram design

Designing the hologram for the sensor presented some challenges. First, the incline angle of the hologram grating had to be large enough to bend and efficiently direct into the air the light coming through the flat glass plate. This angle had to be greater than the critical angle during reconstruction. In construction, one of the two construction waves of the hologram had to meet the conditions for total internal reflection. However, light could not enter from the air, and the hologram could not be created by interference. A hologram exposure method had to be developed that was free of these problems.

We used two-light flux interference exposure and plane waves (see Figs. 4 and 5).

The following symbols are used in this discussion:

- θ_1, θ_2 : Angle of incidence for hologram construction
- θ_3 : Angle of incidence for hologram reconstruction
- θ_4 : Outgoing angle for hologram reconstruction.

If the angle of incidence at the glass surface is θ_{3g}, the scattered light from a fingerprint ridge with upheaval image information will

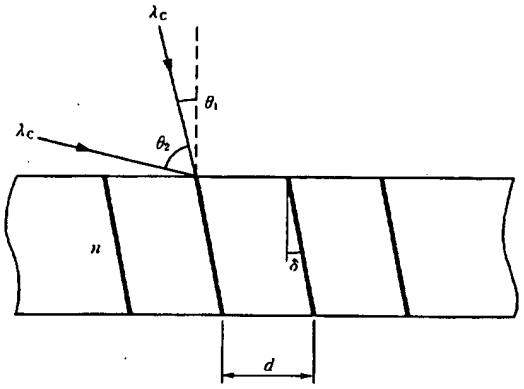

Fig. 4—Angle of incidence for hologram construction.

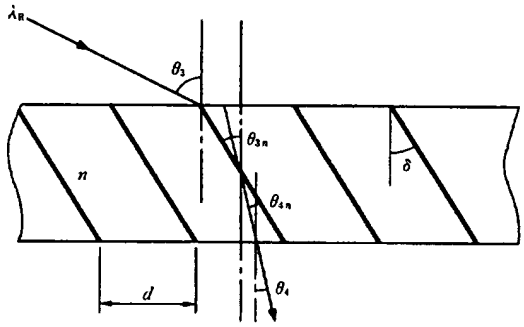

Fig. 5—Hologram reconstruction.

cause total internal reflection at the glass surface of the sensor if the following condition is satisfied:

$$\theta_{3g} > 42°. \quad \ldots\ldots\ldots\ldots (1)$$

Taking the mechanical margin into account, we set the angle of incidence for the prototype sensor to:

$$\theta_{3g} = 45°. \quad \ldots\ldots\ldots\ldots (2)$$

θ_4 for directing scattered light from the glass to the air is 0 degrees because the external image-forming optical system is inlined. That is:

$$\theta_{3g} = 45°, \quad \theta_4 = 0°. \quad \ldots\ldots\ldots (3)$$

When a hologram meeting the above condition is created, interference cannot be used for its construction.

This is because one of the construction waves must enable conditions for total internal reflection in the glass but no light can enter from the air. Adding a trapezoidal prism to holo-

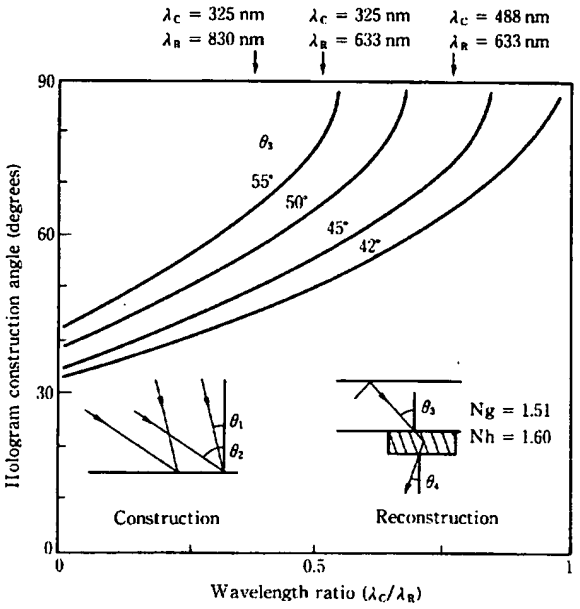

Fig. 6—Relationship between hologram construction angle and wavelength ratio.

gram materials may enable light to enter at an angled surface, but this is hard to achieve.

Therefore, we used light with a wavelength that was λ_C shorter than λ_R for reconstruction as the light source to construct the hologram. This results in a grating inclination angle of δ and a spatial frequency f that meets the conditions for efficient light entry into the air at the critical angle (or wider angle). This enables standard two-light flux interference exposure.

Figure 6 shows the relationship between the angle of incidence for construction and the wavelength ratio. The Y-axis indicates the angle of incidence, θ_1 or θ_2, whichever is larger.

The parameter is the propagation angle, θ_{3g}, of the light that passes through the glass because of total internal reflection in reconstruction. The reconstruction and construction wavelength ratio λ_C/λ_R cannot be made continuous as shown by the arrows in Fig. 6 because the laser wavelength is discrete. If the θ_2 value is too large, hologram exposure optics cannot be implemented, so the value must be as small as possible. Construction wavelength λ_C was made shorter than reconstruction wavelength λ_R to reduce the θ_2 value to less than 90 degrees and to enable light to enter from the air. As θ_{3g}

approaches the critical angle, the θ_2 value becomes small and hologram construction becomes easy. θ_2 also decreases if the construction/reconstruction wavelength ratio λ_C/λ_R decreases. Because the prototype fingerprint sensor uses a He-Cd laser ($\lambda_C = 442$ nm) for hologram exposure and a semiconductor laser for reconstruction ($\lambda_R = 830$ nm), θ_1 and θ_2 were set as follows:

$$\theta_1 = 14.1°, \quad \theta_2 = 54.3°. \quad \ldots\ldots\ldots (4)$$

The spatial frequency f and incline angle δ of the hologram grating then become:

$$f = 1\,286 \text{ lines/mm}, \quad \delta = 21.0°. \quad \ldots (5)$$

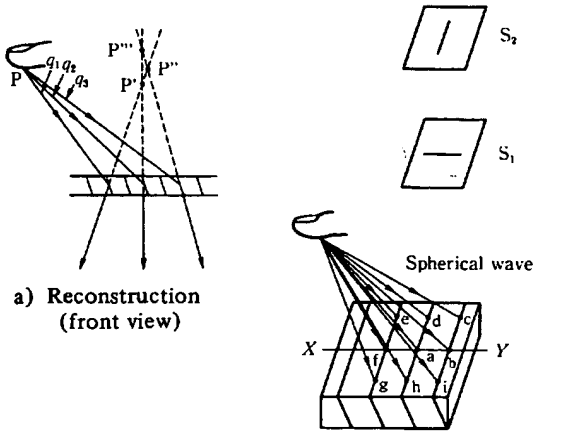

a) Reconstruction (front view)

b) Reconstruction of plain grating by divergent spherical wave (solid figure)

Fig. 7—Cause of astigmatism.

4.2 Designing the image-forming optical system

4.2.1 Astigmatism

As mentioned in section 4.1, the hologram for the fingerprint sensor uses a plane grating created by plane wave interference. Because the light entering the hologram from each point on a fingerprint ridge has a divergent spherical waveform, the virtual image of the fingerprint observed through the hologram has astigmatism.

Figure 7a) shows how astigmatism occurs. At any point on the hologram {Fig. 7b), points a to i}, reconstructed waves do not have the same wavefront as constructed ones. This is because divergent spherical waves scattered by fingerprint ridges are used in reconstruction. The reconstructed wave entering the hologram from point P goes to the image pickup element after being diffracted by the hologram. When diffracted beams q_1, q_2, and q_3 are extended, a virtual image of point P should appear where they cross. However, because the constructed and reconstructed waveforms differ, the three beams cross at points P', P'', and P''' instead of at a single point {see Fig. 7a)}. Because many light paths contribute to the formation of a virtual image, point P on the finger becomes a horizontal stripe (S_1) near the hologram, and becomes a vertical stripe (S_2) at a distance from the hologram {see Fig. 7b)}. Image S_1 is called a vertical virtual image because it is vertically focused. Image S_2 is called a horizontal virtual image because it is horizontally focused.

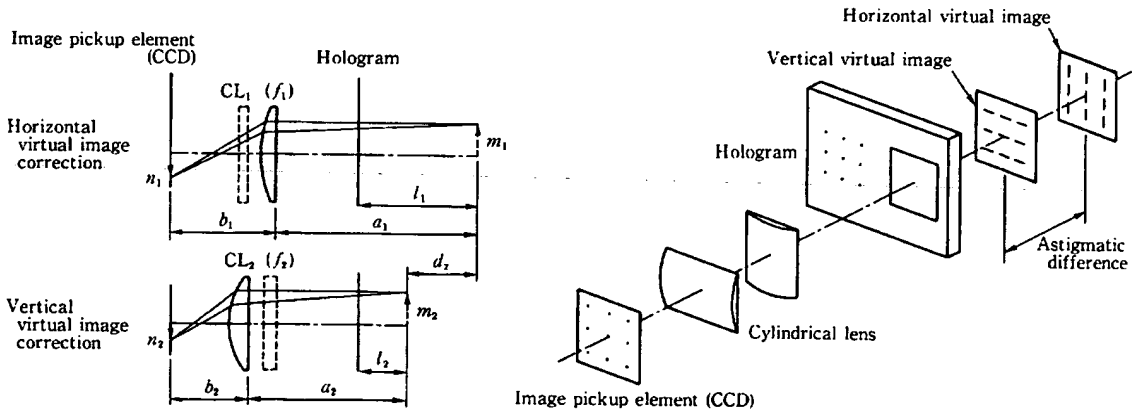

Fig. 8—Astigmatism correction using orthogonal cylindrical lenses.

4.2.2 Orthogonal cylindrical lens

The vertical and horizontal images are best formed independently on the image-forming surface. That is, the lens for vertical images should only contribute to forming vertical images and the lens for horizontal images should only contribute to forming horizontal images. A cylindrical lens is the most suitable for such unidirectional focusing. If two cylindrical lenses are positioned orthogonally, the images can be formed independently (see Fig. 8). Cylindrical lenses CL_1 and CL_2 with focusing distances f_1 and f_2 are used to form the horizontal and vertical image components. If the distances from the image-forming surface to the lenses are a_1 and a_2 and the distances from the lenses to the horizontal and vertical images are b_1 and b_2, the expression below can be derived from the following lens formula:

$$\frac{1}{a_1}+\frac{1}{b_1}=\frac{1}{f_1},\quad \frac{1}{a_2}+\frac{1}{b_2}=\frac{1}{f_2}. \qquad \ldots (6)$$

Because images are formed on the same image-forming surface, the following expression is true when the astigmatic difference is d_z, where

$$d_z=(a_1+b_1)-(a_2+b_2). \qquad \ldots (7)$$

The three expressions below must be satisfied in image formation. If the magnification rates of the horizontal and vertical images are m_1 and m_2, the following expressions are true:

$$m_1=\frac{b_1}{a_1},\quad m_2=\frac{b_2}{a_2}. \qquad \ldots\ldots\ldots (8)$$

a_1, a_2, b_1, and b_2 are deleted from the expressions as follows:

$$d_z=\frac{f_1\cdot(m_1+1)}{m_1}-\frac{f_2\cdot(m_2+1)}{m_2}. \qquad (9)$$

The astigmatic difference, d_z, can be calculated if the distance (optical path length of scattered light) from the finger to the hologram is determined. The magnification rates of the horizontal and vertical images should therefore be set to the desired values to determine the combination of f_1 and f_2.

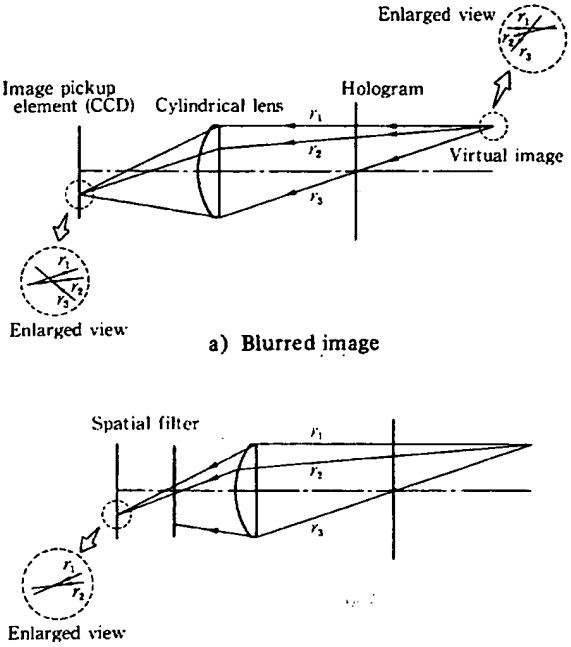

Fig. 9—Improved resolution using spatial filter

So far, only the perpendicular outgoing light from the hologram has been discussed. However, light exiting askew and entering the lens off-axis contributes to form imaging and blurs the image on the image-forming surface {see Fig. 9a)}. To simplify this, only one of the two orthogonal image-forming lenses is shown. Of the light forming a virtual image, all rays (r_1, r_2, and r_3) that pass through the lens contribute to image formation. A new technique is needed to form the entire input pattern clearly on the image-forming surface.

We developed an optical system with a slit spatial filter at the focusing position of the lens, {see Fig. 9b)}. This filter is positioned so that it enables light from r_1 to r_2 to form an image and eliminates light from r_2 to r_3, thus improving resolution. In addition, because all incident light perpendicular to the lens passes the focus point, a spatial filter at this position functions effectively over the entire input area.

Creating an isotropic image in image memory is important for enlarging the identification logical margin so that the fingerprint

a) Touching b) Removed

Fig. 10—Examples of detected fingerprint images.

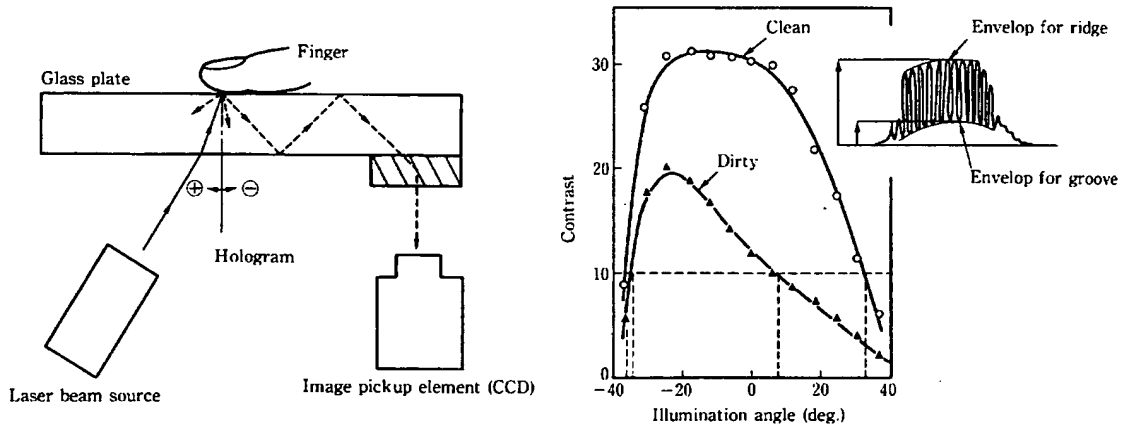

a) Experimental system b) Experiment data

Fig. 11—Relationship between contrast and lighting angle from inside flat glass plate.

can be identified if the finger is turned. In general, the cell spacing of the image pickup element (CCD) is not isotropic. Therefore it is hard to form an isotropic image in memory, and special software and processing time are needed to correct magnification. Vertical and horizontal magnification rates are controlled independently and optical super-parallel operations in holographic sensor optics can quickly and easily produce an isotropic image in memory.

4.3 Optimizing the lighting angle

As mentioned in Chapter 3, the sensor only detects an image formed by scattered light beams from fingerprint ridges. If the input surface is blurred by sweat or grease, light may be reflected and superimposed on the grooves (see Fig. 10). The influence of these latent fingerprints must be eliminated.

Figure 11 shows the relationship between sensor output contrast and the angle of lighting from inside the flat glass plate. Sensor output contrast is defined by the ratio of ridge signal levels to groove signal levels. The lighting angle is plus if it is not on the hologram side of the finger and minus if it is on the hologram side of the finger. The input surface is rated clean immediately after being wiped with isoprophyl alcohol (IPA) and is rated dirty after being

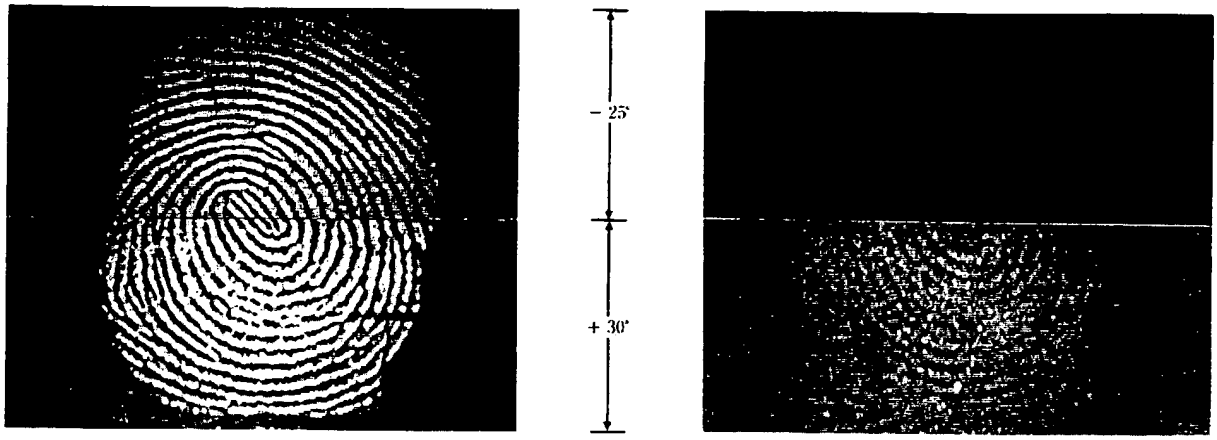

a) Touching b) Removed

Fig. 12—Eliminating the influence of latent fingerprints by optimizing the lighting angle.

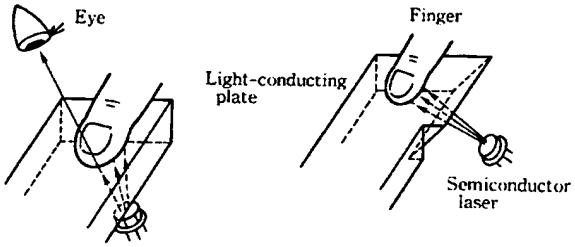

a) Problem of direct lighting method b) Lighting using total internal reflection light

Fig. 13—Ridge selective lighting.

touched by fingers a few times. When the surface was clean, the contrast was almost stable at a lighting angle from −25 degrees to +7 degrees. When the lighting angle was under −25 degrees or over +7 degrees, the contrast deteriorated. This deterioration was probably caused because the light intensity per unit area and the intensity of light that could become internal reflected light from scattered information decreased.

When a fingerprint was entered through a surface blurred with latent fingerprints, the contrast was low at all lighting angles. This was especially so on the plus side. If the contrast is sufficient even when the input surface is blurred (i.e. 10 or more), the lighting angle from inside the glass can be set within the range from −33 degrees to +7 degrees.

Figure 12 compares fingerprint images obtained at lighting angles of −25 degrees and +30 degrees. The image was greatly affected by latent fingerprints when the angle was +30 degrees. However, only the current fingerprint appeared when the angle was −25 degrees.

5. Problems and techniques

5.1 Selective ridge lighting

This holographic fingerprint sensor uses light efficiently because the transparent flat glass plate is lit from directly underneath. This has the disadvantage of light leaking from the fingerprint input port {see Fig. 13a)}. The amount of leakage light is about four times larger than that allowed by laser safety standards. A contact detection mechanism could be installed at the fingerprint input port and the light switched off when not in use. But light would still leak from the sides of the finger when in use. Covering the fingerprint input port would make it uncomfortable to use. To protect the user's eye from the laser beam, the fingerprint sensor must prevent light leaking from the fingerprint input port.

To solve this problem, we developed a ridge-selective lighting system {see Fig. 13b)}. Instead of lighting the transparent flat glass plate from directly underneath, we used a transparent plane plate with a diagonally cut edge through which the light is irradiated.

Figure 14 shows the light leakage at differ-

ent angles. (For the "Clean" result, the glass surface was cleaned with isopropyl alcohol.) The leakage ratio decreases rapidly as the angle of incidence exceeds the critical angle. This is especially true for a clean surface but, even if the surface is dirty, the leakage ratio is only about 9×10^{-3} at 50 degrees of incidence.

The maximum permissible exposure calculated based on IEC Class 1 laser safety standards is 0.18 mW for 830 nm. We use a 25-mW laser diode to obtain a high contrast image. At an angle of incidence of 0 degrees, 0.7 mW would reach an operator's eyes. In our system, a maximum of 0.08 mW reaches the operator's eye, even when the plate is dirty. This more than satisfies the IEC standards.

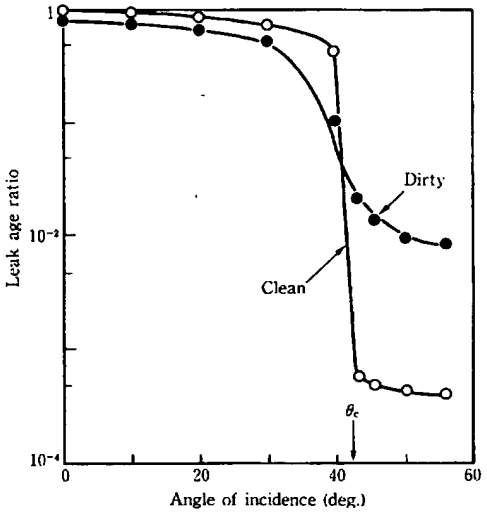

Fig. 14—Leakage ratio as a function of angle of incidence.

5.2 Spatial separation of illuminating light and information light

If the ridge-selective lighting is adopted for safe use of the laser, the lighting angle within the plane perpendicular to the fingerprint input port cannot be optimized as explained in section 4.3.

If the hologram is positioned in a positive reflecting direction from the lighting, a high output will be produced but the scattered beams from latent fingerprints will adversely affect the signal-to-noise ratio. We tried improving the signal-to-noise ratio by: optimizing the detection angle between the light irradiated onto the surface parallel to the fingerprint input surface, and by optimizing the direction in which ridge information light propagates.

Figure 15 shows our experiment and its results. To simplify the experiment, a He-Ne laser ($\lambda = 633$ nm) beam was used for lighting and a prism was used to pick up the light reflected from the finger. To check the relationship between the signal-to-noise ratio and detection angle, the signal-to-noise ratio was defined from: ① the output level S of the scattered light

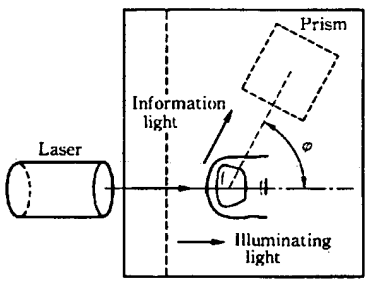

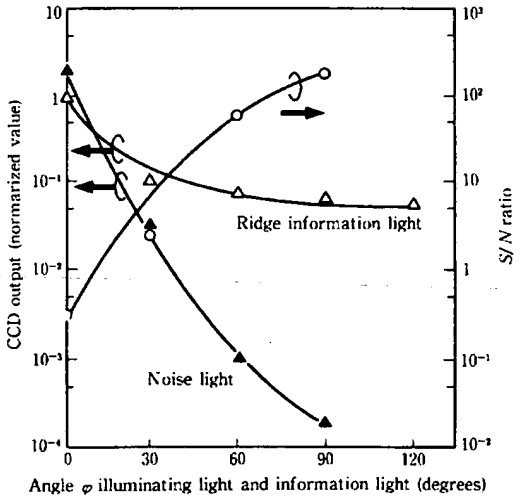

Fig. 15—Relationship between information light S/N ratio and crossing angle of illuminating and information light.

(information light) from fingerprint ridges when a finger was placed on the input surface, and ② from the output level N of the scattered light (noise light) from latent fingerprints with no finger on the input surface. Output level S of ridge information light decreased as detection angle φ increased. However, the signal-to-noise ratio improved because output level N of the scattered light from latent fingerprints decreased faster. The signal-to-noise ratio exceeded 100 when the detection angle was 90 degrees. This means that the influence of latent fingerprints can be ignored. When the detection angle was increased to 120 degrees, output level S of the ridge information light changed little, but output level N of the scattered light from latent fingerprints decreased to almost unmeasurable levels. We finally set the detection angle at 90 degrees to simplify the design and manufacture of the flat glass plate and other mechanical components. At this angle, output level S of the information light from ridges is almost one-tenth that of the regular reflection component. However, this does not cause a problem if the light intensity is correct and optical components use the light efficiently.

5.3 Prototype fingerprint sensor

To verify the effectiveness of the optics explained above, we made a prototype fingerprint sensor (see Fig. 16). It is 230 x 100 x 70 (mm). Figure 17 is an example of these optics using the holographic fingerprint sensor.

Figure 18 shows an example of a detected fingerprint image. A high-resolution image was produced only when a finger was placed on the

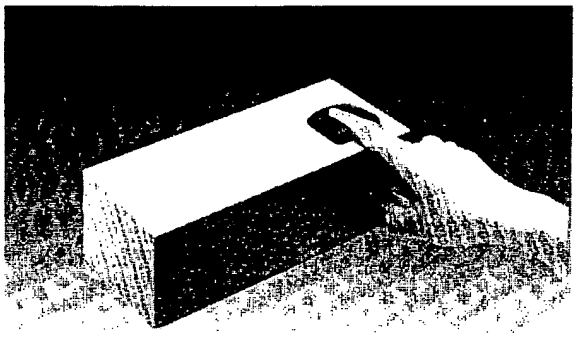

Fig. 16—Prototype fingerprint sensor.

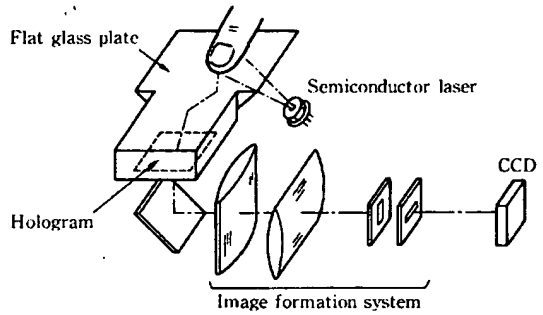

Fig. 17—Plactical optical system of holographic fingerprint sensor.

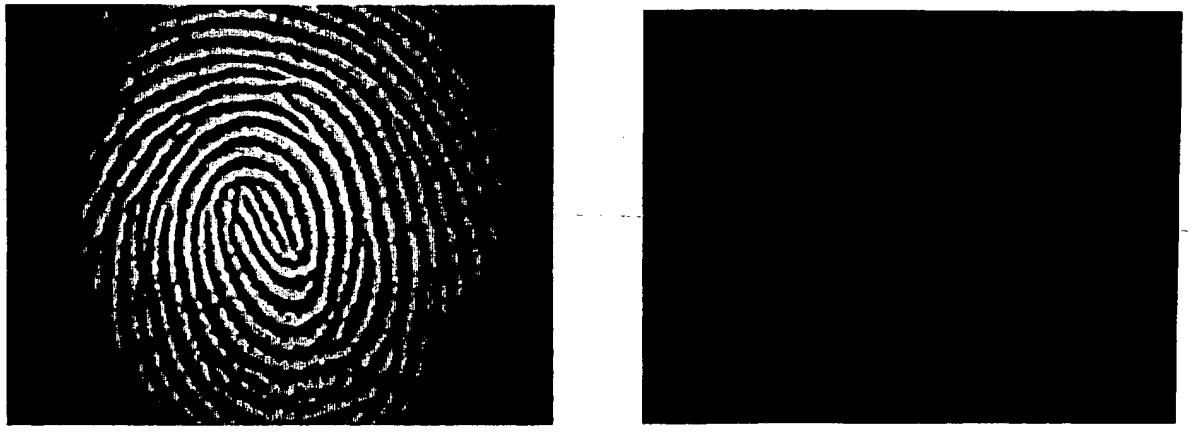

a) Touching b) Removed

Fig. 18—Examples of detected fingerprint images.

fingerprint input port. The scattered black spots in the white ridge lines are sweat glands, proving the sensor's high-resolution.

6. Conclusion

To solve the problem of trapezoidal distortion in conventional real-time fingerprint sensors for personnel identification, we developed a holographic fingerprint sensor consisting of a hologram and a flat glass plate. It uses a parallel-plane plate, so that the distance from each point on the fingerprint to the hologram element is equal and a distortion-free fingerprint image can be obtained. We also developed the hologram and flat glass plate for the sensor and external optics to correct astigmatism caused by the hologram. To make the sensor safe, we introduced ridge-selective lighting, which prevents laser light from leaking from the fingerprint input port and possibly damaging the user's eyes.

If image forming can be integrated into a hologram several micrometers thick together with image pickup, no external optics will be needed, and the system can be made even more compact.

Our next job is to develop a self-image-forming hologram.

References

1) Kawagoe, M., and Tojo, A.: Fingerprint Pattern Classification. *Pattern Recognition*, **17**, 3, pp. 295-303 (1984).
2) Shimizu, A., and Hase, M.: Entry Method of Fingerprint Image Using Prism. (in Japanese), *Trans IECE, Jpn.*, **J67-D**, 5, pp. 627-628 (1984).
3) Igaki, S., Eguchi, S., Ikeda, H., and Inagaki, T.: Realtime Fingerprint Sensor Using a Hologram. Digest Tech. Papers, 1985 Annual Meet., OSA, Washington, DC, p. 78.

Seigo Igaki
Holography and Color-Imaging Laboratory
FUJITSU LABORATORIES, ATSUGI
Bachelor of Electronics Eng.
University of Electro-Communications
1973
Master of Electronics Eng.
Graduate School of Hokkaido University
1975
Specializing in Personal Identification System

Shin Eguchi
Holography and Color-Imaging Laboratory
FUJITSU LABORATORIES, ATSUGI
Bachelor of Electrical Eng.
Keio University 1982
Master of Electrical Eng.
Keio University 1984
Specializing in Holography

Takashi Shinzaki
Holography and Color-Imaging Laboratory
FUJITSU LABORATORIES, ATSUGI
Bachelor of Applied Material Science
Muroran Institute of Technology 1986
Master of Applied Material Science
Muroran Institute of Technology 1988
Specializing in Optical System Design